Design of Sb_2S_3 nanorod-bundles: imperfect oriented attachment

2006 Nanotechnology 17 2098

(http://iopscience.iop.org/0957-4484/17/9/004)

INSTITUTE OF PHYSICS PUBLISHING NANOTECHNOLOGY
Nanotechnology **17** (2006) 2098–2104 doi:10.1088/0957-4484/17/9/004

Design of Sb_2S_3 nanorod-bundles: imperfect oriented attachment

Qifei Lu[1], **Haibo Zeng, Zhenyang Wang, Xueli Cao and Lide Zhang**[1]

Key Laboratory of Materials Physics, Anhui Key Laboratory of Nanomaterials and Nanotechnology, Institute of Solid State Physics, Chinese Academy of Sciences, Hefei 230031, People's Republic of China

E-mail: qflu@issp.ac.cn

Received 24 November 2005
Published 28 March 2006
Online at stacks.iop.org/Nano/17/2098

Abstract
The large scale formation of uniform Sb_2S_3 nanorod-bundles has been achieved via a simple and mild hydrothermal approach with the assistance of polyvinylpyrrolidone. By closely inspecting the growth process and the crystallographic analysis of as-synthesized products, conclusive evidence has been provided to show that the growth mechanism of such nanorod-bundles is imperfect oriented attachment. The anisotropic adsorption of polyvinylpyrrolidone at the different surfaces of Sb_2S_3 nanocrystals assists the one-dimensional preferential growth; it is just the misorientations that result in the nanorod-based superstructures. Moreover, the hydrothermal treatment time plays a crucial role, and can be used as the parameter to control the size and morphology of the bundles. This simple approach promises future large-scale controlled synthesis of various nanobody-based superstructures for many important applications in nanotechnology.

1. Introduction

One-dimensional (1D) nanostructures have attracted great attention in many fields due to their superior electrical, optical, mechanical and thermal properties and potential applications as building blocks in microscale/nanoscale devices [1–3]. With the ongoing development of nanodevices, the direct architecture of complex structures based on 1D nanostructures is believed to be of great significance [4, 5]. So far, various complex nanostructures have been fabricated to achieve the goal of the integration of 1D nanostructures. Recently, Qi *et al* synthesized a cone-like bundle of $BaSO_4$ nanofibres using the double-hydrophilic block copolymers directed mineralization method [6]. Yu *et al* have also prepared funnel-like $BaCrO_3$ and $BaSO_4$ superstructures using a polymer-controlled mineralization reaction [7]. Then, ZnO hierarchical nanostructures with six-, four- and two-fold symmetries have been successfully grown via a vapour transport and condensation technique by Lao *et al* [8]. Using a hydrothermal/solvothermal technique, the groups of Qian and Zeng have also grown several superstructures with novel morphology [9, 10]. Recently, Yuan *et al* successfully synthesized manganese oxide octahedral molecular sieve three-dimensional nanostructures by a hydrothermal method [11]. Sb_2S_3 (with a direct band-gap energy of 1.78 eV) has a chain structure of which be potentially applied in solar energy conversion, thermoelectric cooling technologies and optoelectronics in the IR region [12, 13]. So far, various morphologies and architectures of Sb_2S_3 nanostructures have been reported [14, 15]. However, the controllable synthesis of complex Sb_2S_3 structures with uniform building blocks (e.g. nanorods) is still a challenge. Meanwhile, the growth mechanism of these complex structures has not been sufficiently reported in the literature. Therefore, elucidation of this growth mechanism is another purpose of the present work.

Herein, we synthesized uniform Sb_2S_3 nanorod-bundles on a large scale via a polyvinylpyrrolidone (PVP) assisted hydrothermal process. This synthesis route is mild, reproducible and controllable. The growth mechanism of the Sb_2S_3 bundles, namely imperfect oriented attachment, is of fundamental importance in the design of integrated nanodevices. This procedure also allows morphological and size controlled synthesis by adjustment of the reaction conditions or hydrothermal treatment time.

[1] Authors to whom any correspondence should be addressed.

2. Experimental details

All of the chemicals (analytical grade) were purchased from Shanghai Chemical Reagents Co., Ltd, and were used without any further purification. In a typical procedure, 2.5 g PVP (K30) was mixed with 25 ml deionized water to get PVP sol, then a total of 0.9 g tartaric acid (tart) and 0.46 g antimony trichloride was added to the sol sequentially with constant stirring at 40 °C, then 20 ml thioacetamide solution (0.15 g in deionized water) was introduced dropwise into the mixture. The mixture was transferred into a Teflon-lined autoclave of 50 ml capacity until the mixture became transparent. After the autoclave has been maintained at 180 °C for 20 h, the oven was allowed to cool to room temperature naturally. The resulting products were collected by centrifugation, washed with deionized water and ethanol several times to remove the polymer residues and finally dried at 60 °C for 4 h.

The phase structure and purity of the as-synthesized products was studied by x-ray diffraction using a Philips PW-1710 X'Pert diffractometer with Cu Kα radiation $\lambda = 1.5406$ Å. The morphology and nanostructure of the Sb_2S_3 products were examine by field emission scanning electron microscopy (FE-SEM, Sirion 200), and further studied by transmission electron microscopy (TEM) with a Hitachi H-800 TEM operating at 200 kV. The high-resolution transmission electron microscopy (HRTEM) images and the corresponding selected area electron diffraction (SAED) pattern were taken on a JEOL 2010 HRTEM with energy-dispersive x-ray spectroscopy (EDX) performed at 200 kV. The x-ray photoelectron spectra (XPS) of the products were collected on an ESCALAB MK II x-ray photoelectron spectrometer, using monochromatized Mg Kα radiation as the excitation source.

3. Results and discussions

3.1. Morphology characteristic of Sb_2S_3 bundles

Sb_2S_3 nanorod-bundles were synthesized with the hydrothermal temperature controlled at 180 °C for 20 h. The SEM image reveals that the as-prepared products are predominantly dumbbell-like rod-bundles with a length of 5 μm, as shown in figure 1(a). Further observation reveals that these rod-shaped products are composed of uniform nanorods. The corresponding EDX spectrum taken from the sample is shown in figure 1(b). The curve indicates that these rod-shaped products are composed of Sb and S, and the approximate atomic ratio of Sb to S is about 1:1.5, which suggests to some degree that the samples are Sb_2S_3. The XRD pattern of the products shown in figure 2(a) confirms that the sample is of orthorhombic phase Sb_2S_3 after comparison with the standard pattern from JCPDS 74-1046 for Sb_2S_3 given at the bottom. The chemical state and composition of the as-prepared sample is characterized by its x-ray photoelectron spectrum. Figure 2(b) is an overall XPS survey spectrum and no obvious impurity is detected. The valence state of Sb in the sample is confirmed as Sb^{3+} rather than Sb^{5+}, based on the fact that the binding energies obtained from figure 2(c) (Sb $3d^{5/2}$ 529.3 eV and Sb $3d^{3/2}$ 538.6 eV) are characteristic values of Sb^{3+} instead of Sb^{5+}, which peaks at higher energies [16].

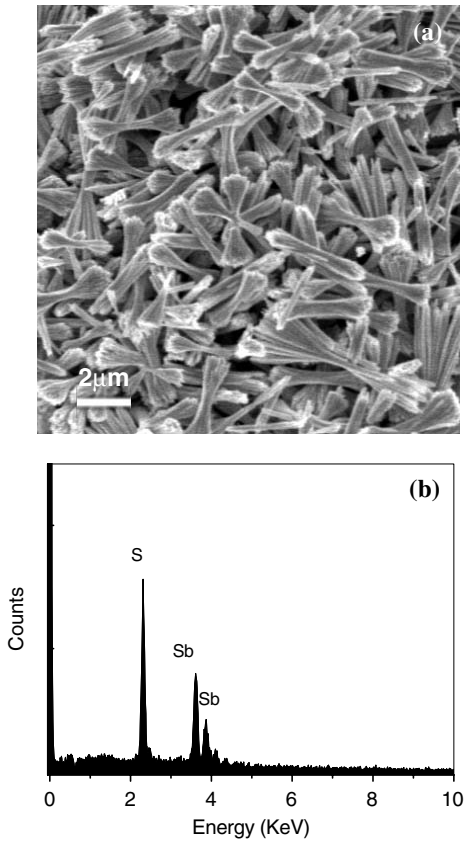

Figure 1. (a) SEM image of the as-synthesized products, showing rod like morphology. (b) EDX spectrum taken from the same sample, showing the composition to be Sb, S.

Further information about the morphology and microstructure of the as-synthesized Sb_2S_3 nanocrystals was obtained using TEM. A low-magnification TEM image of the nanorods is shown in figure 3(a). This reveals that all the dumbbell-like rods-bundles consist of homogeneous nanorods with lengths of about 5 μm and diameters of about 40 nm, and each of them grows three-dimensionally from its centre. The high-magnification TEM image in figure 3(b) shows a nanorod separated from a microstructure. The electron diffraction patterns taken from different positions along the entire length of the nanorod are found to be identical, which reveals the single-crystallinity (see inset in figure 3(b)). Moreover, the electron diffraction suggests that the Sb_2S_3 nanorods grow along the [001] direction, consistent with its chain-like structural features, which leads to 1D growth along the [001] direction. Extensive EDS examinations of a single nanorod show the atomic ratio of S to Sb to be about 1.6:1. All the above SEM and TEM observations suggest that the complex as-synthesized structures are composed of Sb_2S_3 single crystalline nanorods with straight and uniform morphology. The nanorods are about 40 nm in diameter and 5 μm long.

HRTEM has been employed to characterize the detailed microstructure of the products. Figure 4(a) shows the HRTEM image of a single nanorod with a diameter of about 40 nm. The high-magnification HRTEM image and the SAED pattern corresponding to the high-brightness pane are shown in figure 4(b). The spacing between the lattice planes parallel to the nanorod axis is about 0.8 nm, which corresponds to the

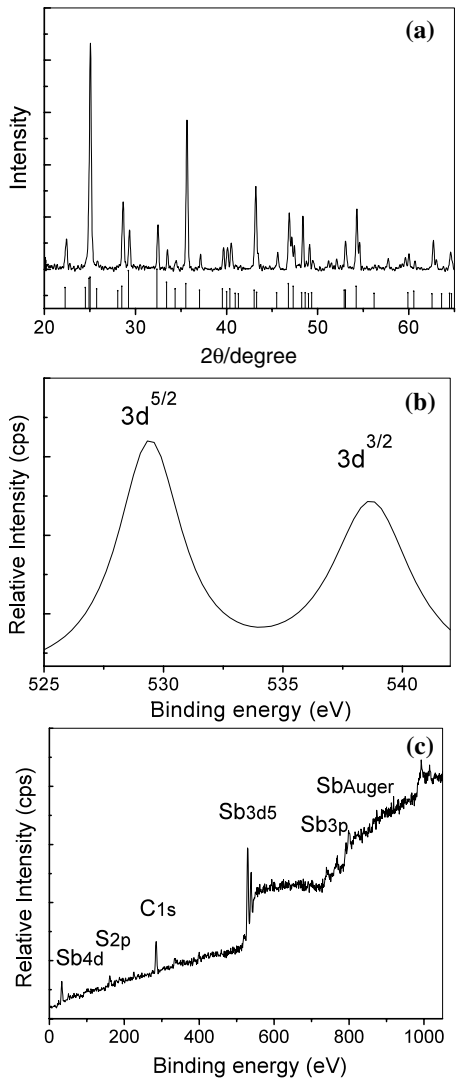

Figure 2. (a) The typical XRD pattern and XPS spectrum of the sample. (b) Sb3d core level. (c) Typical survey spectrum.

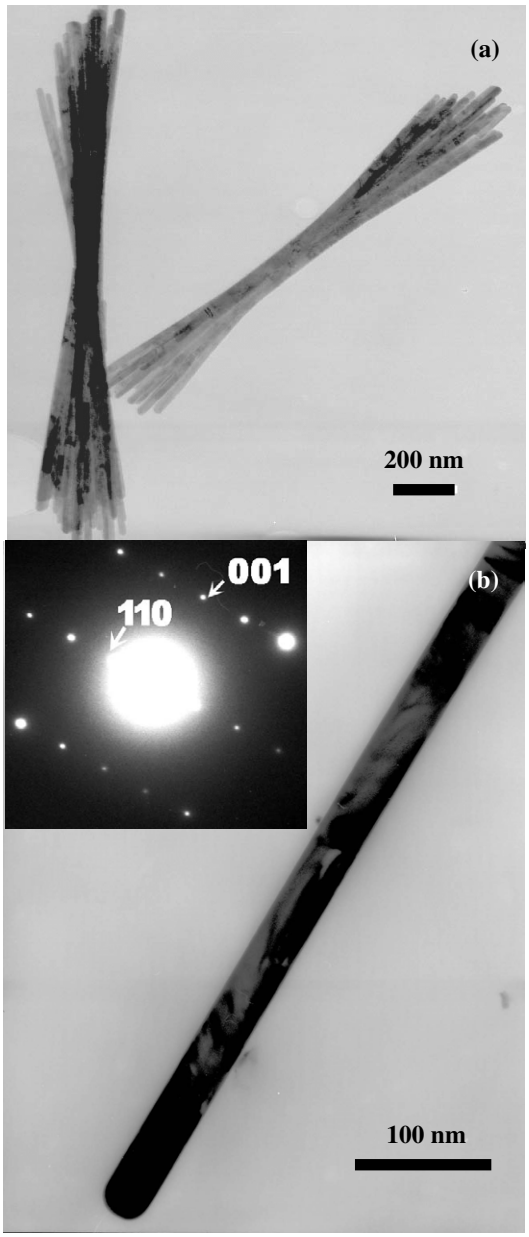

Figure 3. (a) Low-magnification TEM image of nanorod-based bundles and (b) typical high-magnification TEM image of a single nanorod from the bundle. The inset shows the electron diffraction pattern corresponding to the nanorod shown in (b).

distance of two [110] planes of the Sb_2S_3. The results further confirm that the Sb_2S_3 nanorods grow along the [001] direction with good crystallinity.

A field emission (FE) SEM image of two interlaced nanorods with different axis orientations is shown in figure 5(a), and the corresponding TEM morphology is given in figure 5(b). The HRTEM image taken from the area of the white pane marked in figure 5(b) shows clear d_{101} and d_{200} lattice fringes ($d_{200} = 0.357$ nm, $d_{101} = 0.56$ nm). The similar, but not identical, orientation between two attached Sb_2S_3 nanorod axes (1, 2 denote the two attached nanorods, and the interfaces between the rods are marked with arrows) is also shown in figure 5(b), which displays an angle of about 135° between the same d_{101} lattice fringes of the two attached nanorods. The corresponding SAED pattern also confirms the single crystal nature of these attached nanorods.

3.2. Growth mechanism

3.2.1. Imperfect oriented attachment. Large scale self-assembly of nanostructured building components has attracted significant interest for device fabrication as a validated bottom-up technique. Various self-assembly processes based on different driving mechanisms have been proved to be possible [17–20]. Among which, 'perfect/imperfect oriented attachment' has attracted much attention recently as an effective mechanism for fabricating novel complex nanostructures [21–23]. This mechanism is based on self-assembly of primary particles followed by spontaneous adjustment and lattice fusion of the adjacent crystallographic planes, in an ideal case of which the particles are free to move in, for example, liquid or gas environments [24]. Here we report that imperfect oriented attachment (IOA) will result in bundled nanorods in controlled experimental conditions.

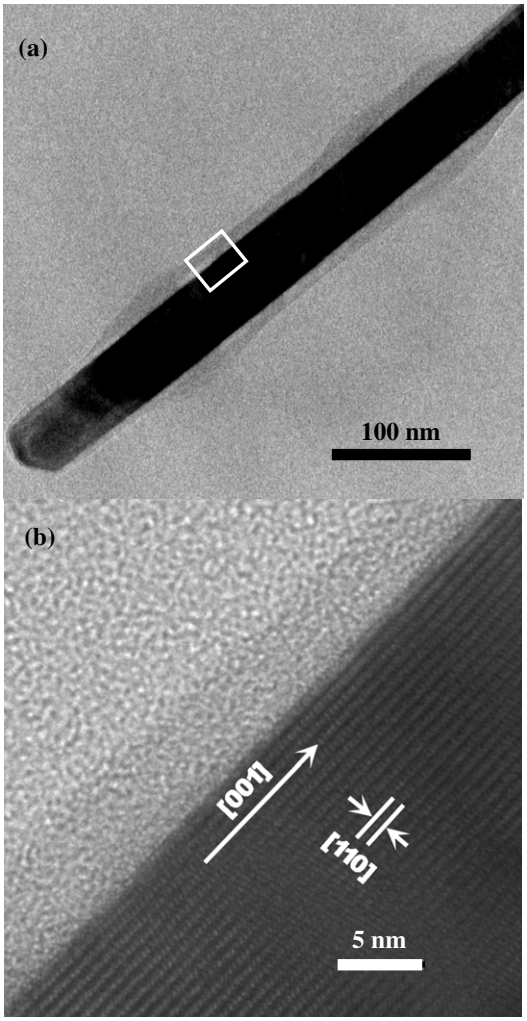

Figure 4. HRTEM image of a single Sb_2S_3 nanorod: (a) low-magnification and (b) high-magnification HRTEM image of a nanorod.

It is believed that the Sb_2S_3 nanobundles in this study are formed mainly via a three-step sequence, i.e. nucleation, self-assembly and 1D growth. The proposed growth mechanism is as follows (see figures 6(a), and (b)).

At the initial stage, amorphous Sb_2S_3 was formed. Under the effect of PVP, much finer amorphous Sb_2S_3 primary particles are formed instead of aggregating as larger ones. In an acid medium, the possible chemical reactions can be given as follows [25]:

$$\mathrm{Sb(III)} + \mathrm{tart} \rightarrow \mathrm{Sb(III)(tart)}$$

$$\mathrm{CH_3CSNH_2} \rightarrow \mathrm{CH_3CNH^+} + 2\mathrm{H^+} + \mathrm{S^{2-}}$$

$$2\mathrm{Sb(III)(tart)} + 3\mathrm{S^{2-}} \rightarrow \mathrm{Sb_2S} \downarrow + 2\mathrm{tart}.$$

Under hydrothermal conditions, with increasing temperature and pressure, the primary particles undergo a crystallization process. Uniform clusters emerge due to a spontaneous self-assembly process among the particles, as a result of van de Waals attraction. Subsequently, oriented attachment will occur after the adjacent nanocrystals adjust their orientation due to the demands of energy minimization. However, the nanocrystal surfaces are not regarded as atomically flat and other vicinal particles will affect the process mentioned above; misorientations therefore remain among the attached nanocrystals.

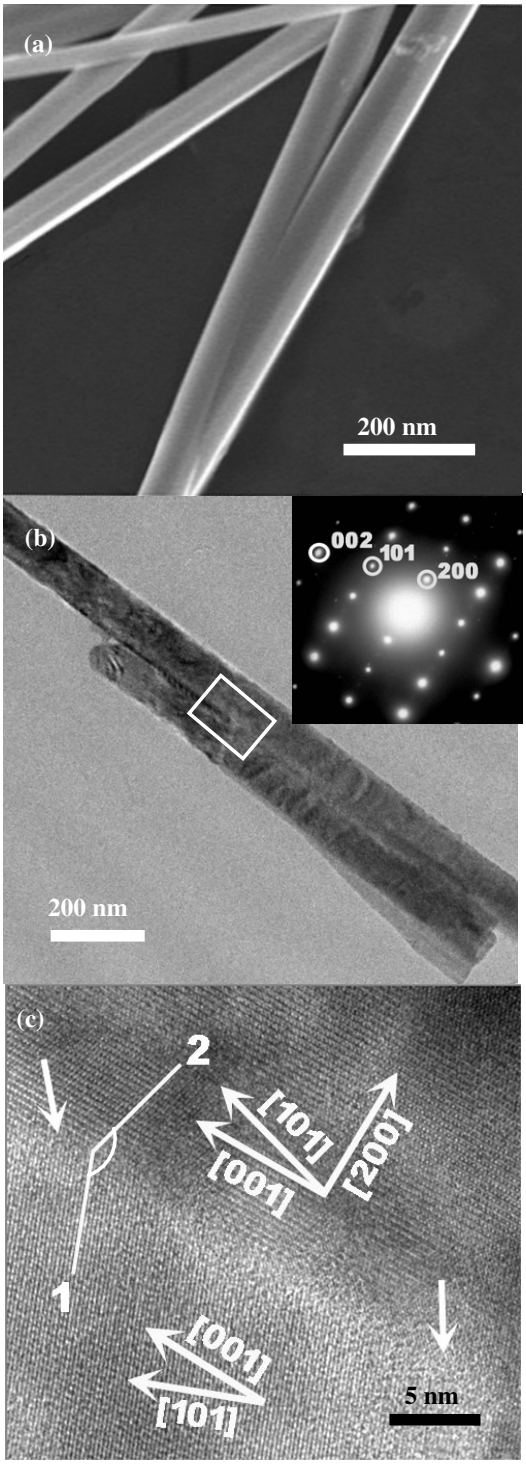

Figure 5. (a) FESEM image of the case two nanorods attached with a small misorientation. (b) Low-magnification HRTEM. (c) High-magnification HRTEM image of attached nanorods, corresponding to the brightness pane in (b). The inset is the corresponding SAED pattern.

Finally, crystalline Sb_2S_3 with an orthorhombic phase is composed of chain-like building blocks along the [001]

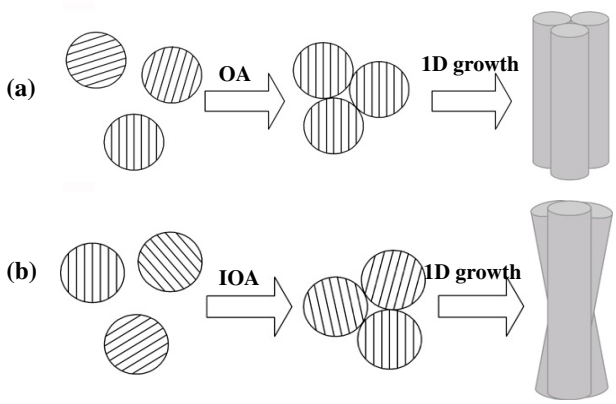

Figure 6. Scheme of the oriented attachment mechanism in hydrothermal conditions: perfect oriented attachment and imperfect oriented attachment are shown in (a) and (b), respectively.

direction; such structural features lead to the formation of anisotropic structures. As discussed in the following section, different surfaces of anisotropic nanocrystalline Sb_2S_3 possess different abilities to adsorb PVP, which in turn help one-dimensional growth along the [001] direction and prevent side-ripening. Thus the attached primary particles can grow into nanorod-bundles with the assistance of PVP. The misorientations results in assembly as an interlaced nanorod-based superstructure but not a parallel nanorod-based superstructure.

The following experiments can validate our proposition: (1) when the temperature is lower than 150 °C, only orange–red amorphous Sb_2S_3 nanoparticles were formed with a narrow size distribution; (2) as discussed later, only inhomogeneous micro- and nanosized rods were found without the assistance of PVP. Figure 5(a) gives a general SEM morphology of the attached nanorods, according to which a small misorientation between axes of the two nanorods can be clearly recognized. If only oriented attachment dominated the formation process, the small misorientation cannot be explained [24]. This is strong evidence, therefore, that the IOA mechanism must dominate the formation of nanorod-based bundles. The IOA mechanism was further confirmed by HRTEM analysis. This can be seen clearly in figure 5(b), which shows that the nanorods are separated by the gap; the connection between the [110] planes of the two nanorods (as indicated by the white square) is further confirmed by the HRTEM image given in figure 5(c). The interface between two nanorods is indicated by two white arrows, and the high-magnification TEM image illustrate that the attached nanorods cannot be parallel to each other due to their misorientation. Therefore, the results further confirm the dominant featrre of the IOA mechanism.

3.2.2. Effect of PVP and hydrothermal treatment time. A series of experiments were performed to study the effect of PVP. If no PVP was added, and the other conditions remain unchanged, the products mainly consisted of inhomogeneous short rods. As shown in figure 7(a) and its inset, the inhomogeneous short rods are attached to each other to form random clusters with a variable shape. With the addition of 2.5 g PVP, the final products mainly consisted of clusters with

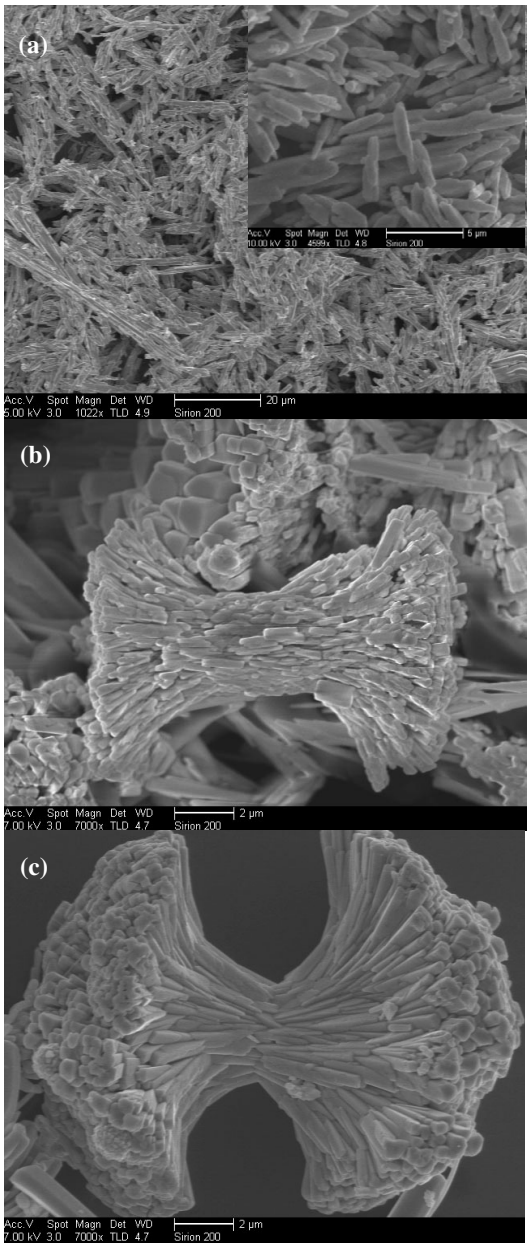

Figure 7. As-synthesized products prepared with various amounts of added PVP: (a) no PVP added, (b) 2.5 g PVP, (c) 3.5 g PVP. The inset in (a) is a high-magnification image of the products in the absence of PVP.

a dumbbell-like shape (see figure 7(b)). And the building block, namely the nanorods, show clear crystal facets and an increasing aspect ratio compared with the products without PVP. When the amount of PVP added was up to 3.5 g, a bundle-like morphology based on longer straight nanorods was obtained, as shown in figure 7(c). Accordingly, the addition of 5.0 g PVP resulted in the final products following the typical process described in the experimental details section. These controlled experiments clearly suggest an effect of PVP on the type of 1D growth.

The polymer PVP has been successfully employed in recent years as a stabilizing agent as well as a structure-directing agent for the preparation of gold and silver

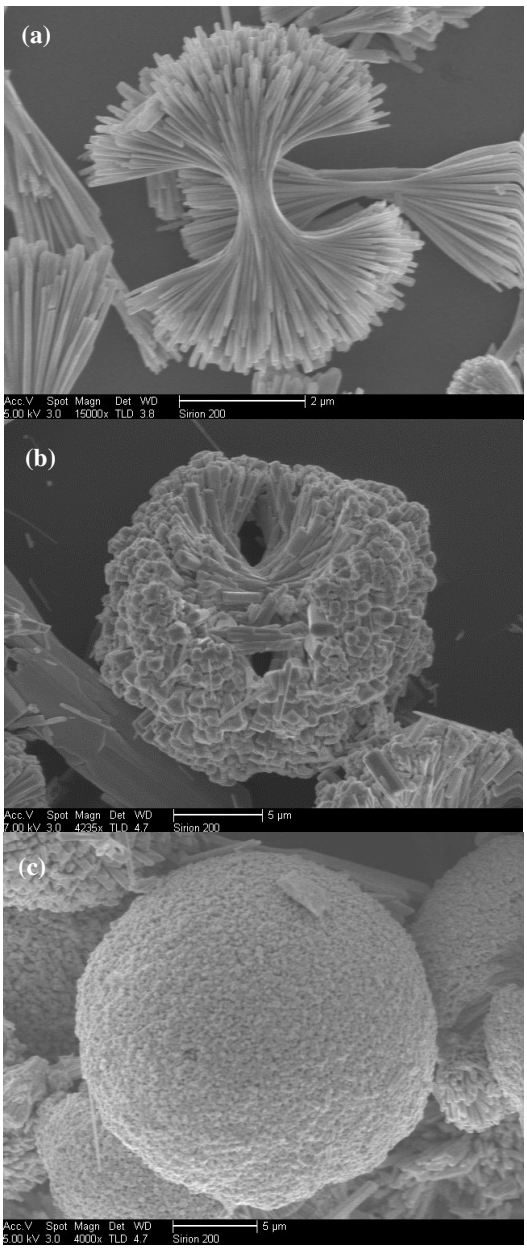

Figure 8. FESEM images of the samples prepared by varying the hydrothermal processing time in the typical synthesis procedure: (a) 25 h, (b) 30 h and (c) 35 h.

nanostructures, including nanowires, nanorods and other novel nanostructures [26, 27]. It is well known that the surfactant PVP prevents the nanoparticles from aggregating due to the steric effect arising from the long polyvinyl chain on the surface of the particles [26]. In this work, PVP was introduced to stabilize the primary particles as well as promote the preferential growth of different crystal planes. In a solution-based processes, crystallographic planes with relatively higher surface free energies are thermodynamically more unstable and easily adsorb capping reagents (i.e. PVP) to reduce their surface free energy. The surface free energy of a specific crystallographic plane (G_{hkl}) may be expressed as $G_{hkl} = \mu_i \times n_{hkl}$, where μ_i is the chemical potential and n_{hkl} is the density of atoms in the [hkl] plane [28]. For the orthorhombic Sb_2S_3, $G_{110} > G_{001}$ due to $n_{110} > n_{001}$ [29], so the [110] plane possesses a greater ability to adsorb capping reagents (PVP) than the [001) plane. In the growth process, PVP is selectively adsorbed on a specific facet, which leads to its preferential growth. In the growth process of Sb_2S_3 bundles, the additive PVP plays a critical role in controlling the size distribution of primary particles at the initial stage as well as the diameter of the obtained nanorod in the bundles. Because the capping effect was largely affected by the fraction of PVP adsorbed on the specific surface of the particles, by adjusting the amount of added PVP the nucleation process as well as the following 1D growth procedure could be controlled.

Furthermore, results obtained with different hydrothermal treatment times during the same procedure present strong evidence for morphological evolution of the bundle-like structures. As shown in figures 8(a)–(c), the morphology of a series of final results suggests that with the elongation of the hydrothermal treatment time, the nanorods in the bundles grow longer. Meanwhile, the IOA mechanism favoured secondary nucleation and growth at the surface of the interlaced part of the as-grown bundle-like nanostructures. New spikes grown from the secondary nucleation points are formed. As the reaction proceeds, the initially formed spikes evolve to nanorods, and finally the closed prickly spheres are formed by these ever-increasing nanorods from the interlaced part. Thus, a morphological evolution from bundle to bowknot-like nanostructures and finally a prickly sphere can be easily understood.

4. Conclusion

In summary, we have synthesized uniform Sb_2S_3 nanorod-based bundles on a large scale via a simple and mild hydrothermal approach assisted with PVP. Conclusive evidence has been provided to illustrate the growth mechanism of Sb_2S_3 nanorod-based bundles. The anisotropic adsorption ability of PVP at the different surfaces of Sb_2S_3 nanocrystals induced the 1D preferential growth, thus resulting in nanorods with a high aspect ratio. Also, the heat treatment time plays an important role and can be used as an additional means to control the size and morphology of the bundles. Taking the Sb_2S_3 as an example, we demonstrate the growth of bundled nanorods and the morphological evolution which follows an imperfect oriented attachment mechanism.

Acknowledgments

This work was financially supported by the National Major Project of Fundamental Research: Nanomaterials and Nanostructures (grant no. 2005CB623603) and the Special Fund for President Scholarship, Chinese Academy of Sciences.

References

[1] Iijima S 1991 *Nature* **354** 56
[2] Yang P D and Lieber C M 1996 *Science* **273** 1836
[3] Dai Z R and Wang Z L 2001 *Science* **291** 1947
[4] Huang Y, Duan X, Wei Q and Leiber C M 2001 *Science* **291** 630
[5] Alivisatos A P 1996 *Science* **271** 933
[6] Qi L M, Cölfen H and Antonietti M 2000 *Angew. Chem. Int. Edn* **39** 604

[7] Yu S H, Antonietti M, Cölfen H and Hartmann J 2003 *Nano Lett.* **3** 379
[8] Lao J Y, Wen J G and Ren Z F 2002 *Nano Lett.* **2** 1287
[9] Zhang R, Chen X Y, Mo M S, Wang Z H, Zhang M, Liu X Y and Qian Y T 2004 *J. Cryst. Growth* **262** 449
[10] Liu B and Zeng H C 2004 *J. Am. Chem. Soc.* **126** 8124
[11] Yuan J K, Li W-N, Gomez S and Suib S L 2005 *J. Am. Chem. Soc.* **127** 14184
[12] Geroge J and Radhakrishnan M K 1980 *Solid State Commun.* **33** 987
[13] Savadogo O and Mandal K C 1992 *Electron. Lett.* **28** 1682
[14] Jiang Y and Zhu Y J 2005 *J. Phys. Chem.* B **109** 4361
[15] Hu H M, Liu Z P, Yang B J, Mo M S, Li Q W, Yu W C and Qian Y T 2004 *J. Cryst. Growth* **262** 375
[16] Karchmer J H 1970 *The Analytical Chemistry of Sulfur and its Compounds* (New York: Wiley) part 1
[17] Yang H G and Zeng H C 2004 *J. Phys. Chem.* B **108** 3492
[18] Yin Y, Rioux R M, Erdonmez C K, Hughes S, Somorjai G A and Alivisatos A P 2004 *Science* **304** 711
[19] Park S, Lim J-H, Chung S-W and Mirkin C A 2004 *Science* **303** 348
[20] Pacholski C, Kornowski A and Weller H 2002 *Angew. Chem.* **114** 1234
[21] Zhang H and Banfield J F 2004 *Nano Lett.* **4** 713
[22] Tang Z, Kotov N A and Giersig M 2002 *Science* **297** 237
[23] Ribeiro C, Lee E J H, Giraldi T R, Varella J A, Longo E and Leite E R 2004 *J. Phys. Chem.* B **108** 15612
[24] Penn R L and Banfield J F 1998 *Science* **281** 969
[25] Desai J D and Lokhande C D 1995 *J. Non-Cryst. Solids* **181** 70
[26] Sun Y G, Gates B, Mayers B and Xia Y N 2002 *Nano Lett.* **2** 165
[27] Mètraux G S, Cao Y C, Jin R C and Mirkin C A 2003 *Nano Lett.* **3** 519
[28] Tiller W A 1991 *The Science of Crystallization: Microscopic Interfacial Phenomena* (New York: Cambridge University Press)
[29] Wyckoff R W G 1964 *Crystal Structure* 2nd edn (New York: Wiley)